The Vulnerable, or High-Risk, Atherosclerotic Plaque:

Noninvasive MR Imaging for Characterization and Assessment[1]

Tobias Saam, MD
Thomas S. Hatsukami, MD
Norihide Takaya, MD, PhD
Baocheng Chu, MD, PhD
Hunter Underhill, MD
William S. Kerwin, PhD
Jianming Cai, MD, PhD
Marina S. Ferguson, MT
Chun Yuan, PhD

"Vulnerable" plaques are atherosclerotic plaques that have a high likelihood to cause thrombotic complications, such as myocardial infarction or stroke. Plaques that tend to progress rapidly are also considered to be vulnerable. Besides luminal stenosis, plaque composition and morphology are key determinants of the likelihood that a plaque will cause cardiovascular events. Noninvasive magnetic resonance (MR) imaging has great potential to enable characterization of atherosclerotic plaque composition and morphology and thus to help assess plaque vulnerability. A classification for clinical, as well as pathologic, evaluation of vulnerable plaques was recently put forward in which five major and five minor criteria to define vulnerable plaques were proposed. The purpose of this review is to summarize the status of MR imaging with regard to depiction of the criteria that define vulnerable plaques by using existing MR techniques. The use of MR imaging in animal models and in human disease in various vascular beds, particularly the carotid arteries, is presented.

© RSNA, 2007

© RSNA, 2007

Radiology

Complications of cardiovascular disease, including stroke, myocardial infarction, and sudden cardiac death, are the most common causes of death in the world (1). Atherosclerotic disease accounts for approximately 25% of ischemic strokes (2) and for the majority of myocardial infarctions and sudden cardiac deaths (3,4). Despite major advances in the treatment of atherosclerosis, a larger percentage of individuals with the disease who are apparently healthy die without prior symptoms (3). The challenge for screening and diagnostic methods is to identify patients at high risk who have lesions that are vulnerable to thrombosis, so-called vulnerable plaques, before the event occurs. To tailor and improve treatment strategies, these screening and diagnostic methods

Essentials

- The challenge for imaging methods is to enable identification of patients with high-risk lesions that are vulnerable to thrombosis, so-called vulnerable plaques, before the occurrence of cardiovascular complications.
- Noninvasive MR imaging has great potential to help characterize atherosclerotic plaque composition and morphology and thus to enable assessment of plaque vulnerability.
- Serial MR imaging of atherosclerotic plaques can provide useful insights on the natural history of vulnerable plaques and might be useful in identifying plaques that are progressing toward a vulnerable state.
- A recent prospective study demonstrated that certain vulnerable plaque features identified on MR images are associated with the occurrence of subsequent cerebrovascular events.
- Most of the plaque imaging data are based on larger vessels, such as the carotid arteries, and further advances in temporal and spatial resolution are needed for coronary plaque imaging.

must be able to help determine the patient-specific risk of experiencing a cardiovascular event.

Imaging methods have the potential to not only be used as a screening tool for the presence of atherosclerosis but also to help distinguish stable from vulnerable plaques and ultimately to distinguish patients with low versus those with high risk of cardiovascular complications. Methods commonly used in atherosclerosis imaging include B-mode ultrasonography (US), intravascular US, conventional angiography, computed tomography (CT), and magnetic resonance (MR) imaging. Each of these imaging modalities has advantages and disadvantages, and all have been reviewed elsewhere (5,6). This article will focus on the particular potential of MR imaging to depict the key features of the vulnerable plaque. MR imaging is well suited for this role because it is noninvasive, does not involve ionizing radiation, enables visualization of the vessel lumen and wall (7,8), and can be repeated serially to track progression or regression. Furthermore, the excellent soft-tissue contrast provided by MR imaging allows evaluation of compositional and morphologic features of atherosclerotic plaques (9–15). This information is crucial because, besides luminal stenosis, plaque composition and morphology are key determinants of a plaque's vulnerability with regard to causing cardiovascular events (3,4).

Authors of several review articles (7,8,16) have described in detail the technical aspects of the MR imaging characterization of human atherosclerotic plaque, including hardware considerations, imaging sequences, and imaging protocols. Results of the accuracy of MR imaging, compared with histologic findings, for measurements of plaque burden, tissue characterization, and fibrous cap status have also been reported (7,8,16). Choudhury et al (7) focused on present and future MR applications for the characterization of atherosclerotic plaques, including real-time vascular intervention, new contrast agents, and molecular imaging.

The present review is a continuation of previous review articles (8,16) and

will focus on the current status of MR as a diagnostic imaging method to help identify the features of vulnerable plaques. The structure of this article is based on two recently published consensus documents (3,4) by a group of experienced researchers in atherosclerosis, including pathologists, clinicians, molecular biologists, and imaging scientists, in which the key features of the vulnerable plaque were defined. The authors of those documents argue that knowledge of luminal diameter is not sufficient to determine the vulnerability of an atherosclerotic lesion, and they propose five major and five minor criteria for the detection of vulnerable plaques. These plaque features were based on studies of coronary arteries and included a thin cap with a large lipid-necrotic core, active inflammation, a fissured plaque, stenosis greater than 90%, endothelial denudation with or without superficial platelet aggregation and fibrin deposition, endothelial dysfunction, calcified nodules, intraplaque hemorrhage, glistening yellow plaques (seen at angioscopy), and outward remodeling (see Table 1).

In this review, we will discuss the role of MR imaging in the identification of each of the features that define the vulnerable plaque, as proposed in the consensus documents (3,4).

Major Criteria

Thin Cap with Large Lipid-Necrotic Core

Virmani et al (17) defined the fibrous cap as a distinct layer of connective tissue completely covering the lipid-necrotic core. The lipid-necrotic core, which is frequently surrounded by macrophages, consists of large amounts of extracellular lipid, cholesterol crystals, and necrotic debris (17,18). Lesions

with a large lipid-necrotic core and a thin fibrous cap are considered to be most likely to rupture (19).

MR imaging is able to help characterize all major plaque components, including the lipid-necrotic core, by depicting particular combinations of signal intensities of each component on images obtained with different contrast weightings (see Table 2 for details). Initial experiments involving ex vivo imaging of endarterectomy specimens by using T1-, T2-, and intermediate-weighted imaging demonstrated that tissue components, including the lipid-necrotic core, hemorrhage, and calcification, could be detected with sensitivities and specificities ranging from 84% to 100% (12). Translation of these findings to in vivo imaging showed that the lipid-necrotic core and intraplaque hemorrhage could be identified with a sensitivity of 85% and a specificity of 92% (20). The ability of MR imaging to demonstrate plaque composition in vivo enables classification of human carotid atherosclerotic plaque, according to criteria developed by the American Heart Association. Cai et al (14) showed that in vivo MR imaging can help identify sections that have either a lesion with a confluent extracellular lipid-necrotic core (American Heart Association type IV lesion) or a lipid-necrotic core covered by a fibrous cap (type V lesion), with a sensitivity of 84% and a specificity of 90%.

While initial studies showed that MR imaging is able to depict the lipid-necrotic core, recent reports have focused on quantifying it. In an ex vivo MR imaging study of carotid endarterectomy specimens by Clarke et al (10), who used diffusion-weighted imaging in addition to T1-, intermediate-, and T2-weighted imaging, pixels were classified into different plaque components and were then compared with histologic specimens. On the basis of this classification, the sensitivity and specificity for necrotic tissue were 83.9% and 75%, respectively. Quantification of the lipid-necrotic core was recently translated to in vivo plaque imaging by using TOF and T1-, T2-, and intermediate-weighted sequences (9). In a study with 40 subjects, a radiologist and a pathologist manually

identified the major components of carotid atherosclerotic plaque on MR images and serially sectioned carotid endarterectomy specimens, respectively (Fig 1). MR measurements of the lipid-necrotic core did not differ significantly from findings on histologic specimens (23.7% vs 20.3%; $P = .1$), and a strong correlation between MR and histologic area measurements was found ($r = 0.75; P < .001$) (9).

Comparison of T1-weighted images obtained before and after contrast material enhancement may improve the accuracy of MR for differentiating the lipid-necrotic core from surrounding fibrous tissue. The lipid-necrotic core shows little if any enhancement on postcontrast T1-weighted images, and differentiation from the surrounding enhancing fibrous tissue is thereby facilitated (21). Using pre- and postcontrast T1-weighted images, Cai et al (22) showed that the lipid-necrotic core, measured as proportion of the vessel

wall, was similar on MR images and histologic specimens, with values of 30.1% ± 12.5 (standard deviation) and 32.7% ± 12.3, respectively. Furthermore, area measurements were strongly correlated ($r = 0.85; P < .001$).

The ability of MR imaging to help determine the status and thickness of the fibrous cap will be discussed in the following section.

Fissured Plaque

Virmani et al (17) described plaque rupture as an area of fibrous cap disruption whereby the overlying thrombus is in continuity with the underlying lipid-necrotic core. Typically, these lesions have a large lipid-necrotic core and a disrupted fibrous cap infiltrated by macrophages and lymphocytes; smooth muscle cell content within the fibrous cap at the rupture site may be sparse (17).

Hatsukami et al (15) reported the use of a three-dimensional TOF bright-

---

Table 1

Criteria for Defining Vulnerable Plaques on the Basis of the Study of "Culprit" Plaques

Type of Criteria	Criterion
Major	Active inflammation: monocyte and macrophage and sometimes T-cell infiltration
	Thin cap with large lipid-necrotic core
	Endothelial denudation with superficial platelet aggregation
	Fissured plaque
	Stenosis >90%
Minor	Superficial calcified nodule
	Glistening yellow plaque seen at angioscopy
	Intraplaque hemorrhage
	Endothelial dysfunction
	Outward (positive) remodeling

Figure 1
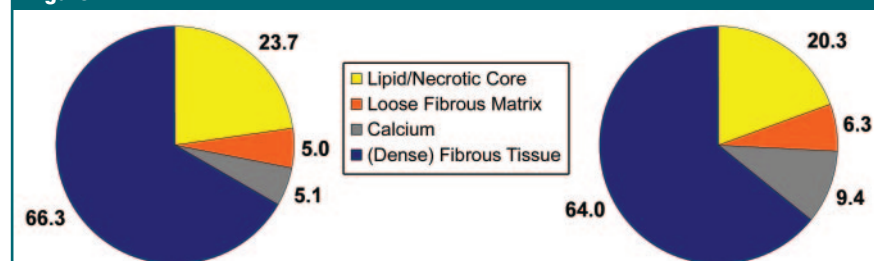
Figure 1: Pie charts show plaque composition as percentage of vessel wall area, calculated per artery and then averaged across all arteries, for MR imaging and histologic specimens. Percentages were compared by using paired *t* tests. (Reprinted, with permission, from reference 9.)

Radiology

blood imaging technique (multiple overlapping thin slab angiography, or MOTSA [23]) to help identify a ruptured fibrous cap in atherosclerotic human carotid arteries in vivo. By using preoperative images of 22 consecutive endarterectomy patients, the in vivo state of the fibrous cap was characterized on the basis of its appearance on MR images as being intact and thick, intact and thin, or ruptured (Fig 2). The authors found a high level of agreement between the MR findings and the histologic state of the fibrous cap, with Cohen κ = 0.83 (95% confidence interval = 0.67, 1.00) and weighted κ = 0.87. An MR investigation by Mitsumori et al (24) demonstrated that in vivo MR imaging has high test sensitivity (81%) and specificity (90%) for the identification of a thin or ruptured cap. Trivedi et al (25) used a short-tau inversion-recovery sequence to quantify the fibrous cap and lipid-necrotic core of 25 recently symptomatic patients and correlated the results with the excised carotid endarterectomy specimens. The authors showed good agreement between MR and histologic quantifications of both the fibrous cap and the lipid-necrotic core content, with good interobserver agreement (intraclass correlation coefficients of 0.88–0.94) (25). Kramer et al (26) studied aortic atherosclerotic plaques in 23 patients with abdominal aortic aneurysm by using T1- and T2-weighted black-blood spin-echo sequences and gadopentetate dimeglumine–enhanced T1-weighted images. The κ value for agreement between the number of tissue components demonstrated by MR imaging and identified at pathologic examination was 0.79. These components included the fibrous cap, thrombus, and/or the lipid-necrotic core. The authors found that contrast enhancement improved the delineation of the fibrous cap, which was found to be hyperintense relative to the lipid-necrotic core on T2-weighted images. Wassermann et al (27), in a study of nine subjects with carotid atherosclerosis, found that gadolinium-enhanced T1-weighted images helped discriminate

Table 2

MR Parameters in Selected Studies

Setting*	Magnet (T)	Contrast Weighting†	Contrast Agent‡	Voxel Size (μm)
Human carotid (13)	1.5	Dual-echo T2 (R-R interval/20, 55), T1 (500/18)	None	$390 \times 390 \times 5000$
Ex vivo human carotid (12)	9.4	Intermediate to T2 (1000–2000/13–50), T1 (300–700/13)	None	$256 \times 256 \times 500$
Human carotid (15)	1.5	3D multiple overlapping thin-slab MR angiography (34 or 22/2.9–4.4)	None	$510 \times 510 \times 1000$
Dogs (42)	1.5	3D T1 (24/8.1), 3D phase-contrast MR angiography (15/5.3)	Fibrin-targeted nanoparticle	Not applicable
Rabbit aorta (54)	1.5	3D MR angiography (6.7/1.6)	USPIOs	$1100 \times 1000 \times 1400$
Human coronary arteries (62)	1.5	3D MR angiography (2.4/8.8)	None	$700 \times 1000 \times 1500$
In vitro human carotid (11)	2.0	T2 (2000/50)	None	$117 \times 117 \times 1500$
Human coronary arteries (103)	1.5	3D black-blood spiral acquisition (30/2)	None	$1000 \times 1000 \times 1000$
Swine carotid (37)	1.5	T1 (700/11), T2 (2000/42)	None	$470 \times 470 \times 3000$
Human carotid and aorta (101)	1.5	Intermediate (2 R-R intervals/12), T2 (2 R-R intervals/45)	None	469^2–$780^2 \times 3000$
Ex vivo human carotid (10)	1.5	T1, T2, intermediate, diffusion-weighted, fast imaging employing steady state (see reference 10 for details)	None	$156 \times 156 \times 200$
Rabbit aorta (56)	1.5	T1 (380/11)	$\alpha_v\beta_3$-integrin–targeted nanoparticles	$250 \times 250 \times 5000$
Human carotid (55)	1.5	T1 (41–44/8.0–9.2), T2* (R-R interval/20), intermediate (2–3 R-R intervals/20)	USPIOs	$208 \times 256 \times 5000$
Human carotid (86)	1.5	T1 turbo spin echo (900/10.3), T1 turbo field echo (570/14)	None	$390 \times 490 \times 2500$
Human aorta (27)	1.5	T1 breath hold (R-R interval/32), T2 breath hold (2 R-R intervals/80)	None	$1210 \times 620 \times 7000$
Swine coronary arteries (43)	1.5	3D turbo field echo (3.8/1.9), 3D inversion recovery MR angiography (4.7/1, inversion time, 4 msec)	Fibrin-targeted agent	$1250 \times 1250 \times 3000$
Human coronary arteries (64)	1.5	Whole-heart 3D steady-state free precession MR angiography (4.7–31/1.7–2.3)	None	$700 \times 1000 \times 3000$
Human carotid (9)	1.5	T1 (800/9.3–11), intermediate to T2 (3–4 R-R intervals/10–70), 3D TOF (23/3.5)	None	$600 \times 600 \times 2000$
Human aorta (104)	1.5	Intermediate (2 R-R intervals/10), T2 (2 R-R intervals/60)	None	$780 \times 780 \times 5000$
Human carotid (49)	1.5	Two-dimensional T1 spoiled gradient-recalled echo (100/3.5)	Gadolinium chelate	$600 \times 800 \times 3000$
Human carotid (22)	1.5	Enhanced and unenhanced T1 (800/9.3–11)	Gadolinium chelate	$600 \times 600 \times 2000$

* Except where otherwise noted, studies were in vivo. Number in parentheses is the reference number.

† Data in parentheses are repetition time msec/echo time msec. TOF = time of flight, 3D = three-dimensional.

‡ USPIO = ultrasmall paramagnetic iron oxide.

Figure 2
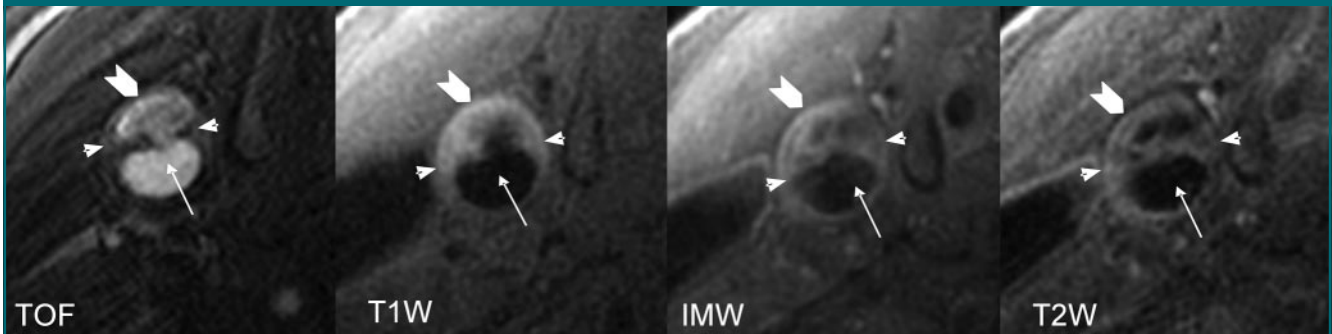
Figure 2: Transverse MR images depict fibrous cap rupture (arrows) in right common carotid artery. The hyperintense region (chevron) on TOF (repetition time msec/echo time msec, 23.0/3.8) and T1-weighted *(T1W)* (800/9.3) images and hypointense region on intermediate-weighted *(IMW)* (2500/10.0) and T2-weighted *(T2W)* (2500/39.9) images is a lipid-necrotic core with type I hemorrhage. Parts of remaining fibrous cap (arrowheads) are visible on TOF image.

the fibrous cap from the lipid-necrotic core, with a contrast-to-noise ratio as good as or better than that of T2-weighted MR images but with approximately twice the signal-to-noise ratio (postcontrast images, 36.6 ± 3.6; T2-weighted images, 17.5 ± 2.1; $P < .001$). Cai et al (22) used unenhanced T1-weighted and contrast-enhanced T1-weighted images to measure the intact fibrous cap. The authors showed moderate to good correlation between findings from carotid MR imaging and the excised histologic specimen for maximal thickness ($r = 0.78$, $P < .001$), length ($r = 0.73$, $P < .001$), and area ($r = 0.90$, $P < .001$) of intact fibrous cap.

Yuan et al (28) used three-dimensional TOF and intermediate-, T1-, and T2-weighted images in 28 symptomatic and 25 asymptomatic subjects to determine whether fibrous cap thinning or rupture, identified on MR images, is associated with a history of recent transient ischemic attack or stroke. Compared with patients with a thick fibrous cap, patients with a ruptured cap were 23 times more likely to have had a recent transient ischemic attack or stroke (95% confidence interval: 3, 210) (28).

Endothelial Denudation with Superficial Platelet Aggregation and Fibrin Deposition

Atherosclerotic plaques with endothelial denudation are characterized either by superficial erosion and platelet aggregation or by fibrin deposition (17). Platelet aggregation may lead to luminal occlusion and acute cardiovascular events, or platelets may layer and organize, further contributing to plaque progression (17,29). In this section, we will discuss the ability of MR imaging to help identify platelet aggregation or fibrin deposition. (The ability of MR to help evaluate endothelial denudation or dysfunction will be discussed in the section Endothelial Dysfunction.)

The detection of thrombus and the determination of its age on MR images are mainly related to the physical characteristics and visual appearance of thrombus (30), which originate from the cross linking of the fibrin strands, thrombus organization (31), the structure of hemoglobin, and the oxidation state (32). Toussaint et al (31) used the water diffusion properties of atherothrombotic tissue to distinguish fresh thrombi from 1-week-old thrombi and occluding old thrombi on MR images. Recently, a similar technique (diffusion-weighted MR) was successfully applied for the detection of cerebral venous thrombosis (33) and dural sinus thrombosis (34). Gradient-recalled-echo MR imaging is frequently applied in the study of cerebral hematoma and venous thrombosis (35).

Corti et al (36) demonstrated the potential of black-blood MR imaging (T1 and T2 weighted) for help in the detection of thrombus and thrombus age in pigs. Thrombi induced in the carotid arteries were monitored at 6 hours; 1 day; and 1, 2, 3, 6, and 9 weeks. Temporal changes due to thrombus organi-

zation were clearly depicted on T1- and T2-weighted MR images and were expressed as alterations in signal intensity relative to the signal intensity of adjacent muscle. Authors of another study (37) showed the potential of gadolinium-enhanced MR imaging to help discriminate different types of intracardiac clots (subacute and organized) in the cardiac chambers in 15 patients scheduled for cardiotomy.

Kampschulte et al (38) used an in vivo multisequence protocol (TOF and intermediate-, T1-, and T2-weighted imaging) in 26 patients scheduled for carotid endarterectomy, to differentiate between intraplaque hemorrhage (Fig 3a) and juxtaluminal hemorrhage/thrombus (Fig 3b). For locations in which MR and histologic findings were in agreement regarding the presence of any type of hemorrhage, MR imaging enabled differentiation of juxtaluminal hemorrhage and thrombus from intraplaque hemorrhage with an accuracy of 96%, with histologic findings as the reference standard. This technique was used to evaluate whether in vivo MR imaging can depict differences between symptomatic and asymptomatic carotid atherosclerotic plaques in the same patient at the same point in time (39). Compared with asymptomatic plaques, plaques associated with neurologic symptoms were associated with a higher occurrence of juxtaluminal hemorrhage and thrombus (61% vs 26%; $P = .039$), whereas intraplaque hemorrhage was common in both symptom-
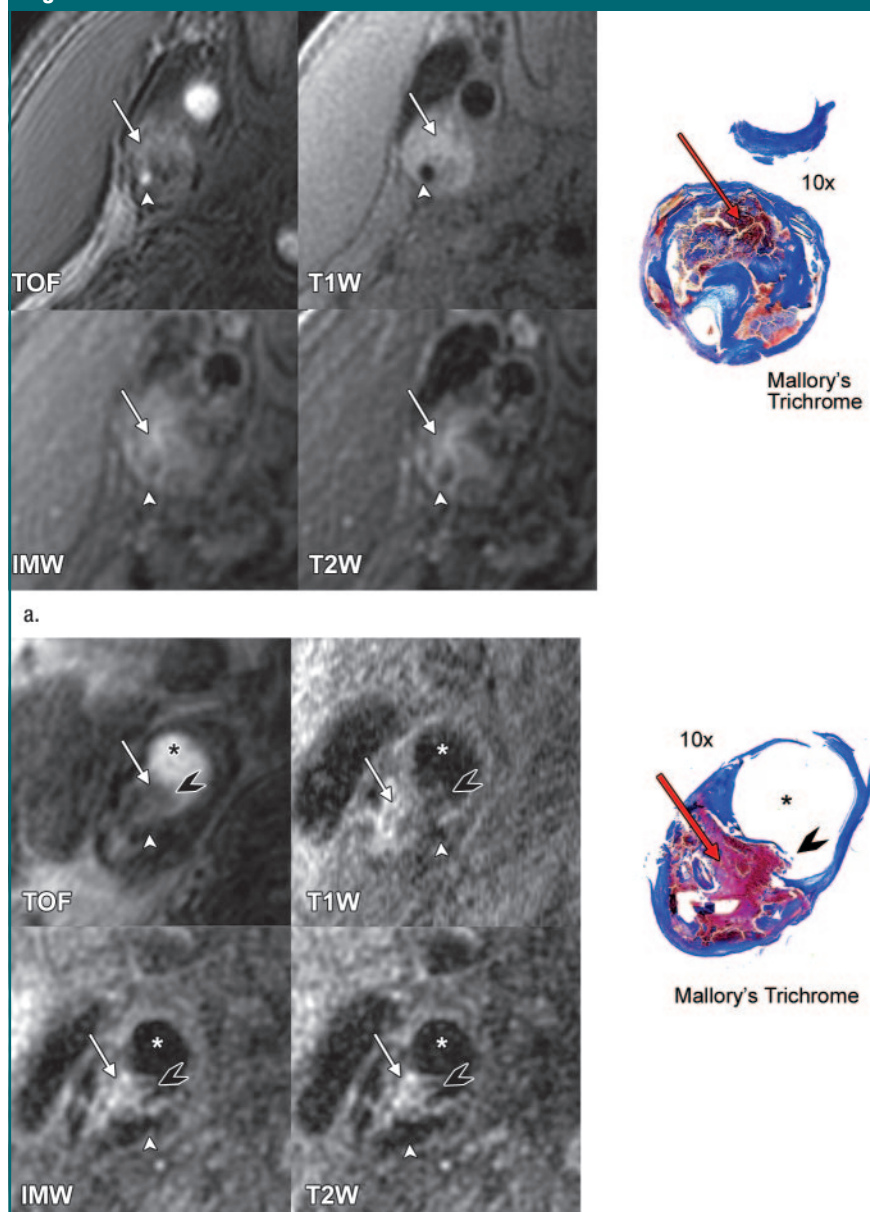
Radiology

atic and asymptomatic plaques (91% vs 83%; $P = .5$).

New targeted contrast agents to enable detection of local small thrombi are under development (30). Fibrin can be identified by using lipid-encapsulated perfluorocarbon paramagnetic nanoparticles in vitro (40,41) and in vivo

(41). Botnar et al (42) used a fibrin-binding gadolinium-labeled peptide in an experimental rabbit model of plaque rupture and thrombosis to detect acute and subacute thrombosis. Similar agents have been successfully used in swine to detect coronary thrombus and in-stent thrombosis (43), as well as pulmonary emboli (44).

Active Inflammation

Inflammation plays a critical role in plaque initiation, progression, and disruption and represents an emerging target in the treatment of atherosclerosis (45). Systemic indicators of inflammation such as C-reactive protein and interleukin-6 titers can be easily obtained by testing blood samples, and it has been shown that a variety of circulating inflammatory markers are associated with the risk of coronary artery disease (45). However, it appears unlikely that C-reactive protein or any of the other markers actually causes the disease (45). Instead, they reflect the local inflammatory process in the artery and perhaps other tissues (eg, adipose tissue) (45). It is this local inflammatory process that can be assessed by noninvasive imaging methods.

Plaques with active inflammation may be identified by the presence of extensive macrophage accumulation (46), and recent investigations with MR imaging have shown an association between contrast enhancement and the degree of macrophage infiltration of plaque (47,48). Lin et al (49) were, to our knowledge, the first to use gadolinium-based contrast agents in atherosclerotic plaque imaging in an animal model, and they demonstrated strong contrast enhancement of the vessel wall. Lin et al concluded that the contrast enhancement of the vessel wall that they observed was caused by an increased vascular supply associated with thrombosis and neointimal thickening. Aoki et al (50) used dynamic MR imaging to correlate carotid wall enhancement changes with pathologic conditions. The dominant feature they noted was a bright outer rim of the vessel wall, which was attributed to growth of the vasa vasorum in the adventitia.

Figure 3

a.

b.

Figure 3: **(a)** Left: Transverse TOF (23/3.8), T1-weighted *(T1W)* (800/9.3), intermediate-weighted *(IMW)* (3488/20), and T2-weighted *(T2W)* (3488/40) MR images depict intraplaque hemorrhage (arrows) deep within highly stenosed carotid plaque with smooth luminal surface. Arrowheads = lumen. Right: Endarterectomy specimen. **(b)** Left: Transverse TOF (23/3.8), T1-weighted *(T1W)* (550/9), intermediate-weighted *(IMW)* (3093/20), and T2-weighted *(T2W)* (3093/40) MR images depict juxtaluminal hemorrhage/thrombus (arrows) adjacent to the lumen (∗), with luminal surface irregularity (chevrons). A calcified area (arrowheads) is hypointense on MR images obtained with all four contrast weightings. Right: Endarterectomy specimen. (Reprinted, with permission, from reference 38.)

Radiology

Yuan et al (21) used contrast-enhanced T1-weighted images and found the greatest enhancement to be associated with areas of dense neovasculature, which are thought to contribute to plaque destabilization (51).

An advantage of using contrast agents that is only beginning to be explored in plaque imaging is the ability to extract quantitative measurements of enhancement. To date, such studies have focused on the use of kinetic modeling and dynamic contrast-enhanced MR imaging to measure the rate of enhancement. Kerwin et al have identified a fast enhancement component, v_p, associated with plaque neovasculature (47) and a slower enhancement component, K^{trans} (Fig 4), associated with permeability (48). It has recently been demonstrated (48) that these dynamic enhancement parameters are strongly associated with macrophage density in advanced carotid plaque (Fig 4). Macrophage density was estimated from histologic specimens by using software (Image-Pro Plus; Media Cybernetics, Bethesda, Md) to measure the total area that stained positive for macrophages and normalizing according to the plaque cross-sectional area (48).

An alternative method for imaging macrophage content is to use ultrasmall superparamagnetic iron oxide (USPIO) particles that are suspended in solution and injected into patients. USPIOs alter MR reaction times, and the propensity of macrophages to phagocytose the USPIOs results in USPIOs being a macrophage-specific agent (52). If sufficient time for macrophage uptake is allowed—at least 24 hours—T2*-weighted images show substantial signal intensity reduction due to the susceptibility effects of USPIOs (53). In experiments with human carotid endarterectomy subjects, Kooi et al (54) showed that macrophages within plaques were positive for iron at histologic and electron microscopy evaluations of endarterectomy specimens. On MR images of corresponding locations, substantial signal intensity reductions were observed.

αvβ3-Integrin is a molecule that is believed to be associated with angiogenesis and inflammation. An αvβ3-integrin–targeted agent was shown to yield greater enhancement in cholesterol-fed rabbits than in controls, and cholesterol-fed rabbits also exhibited increased development of the adventitial vasa vasorum (55).

Severe Stenosis

Arterial stenosis is an abnormal narrowing of a blood vessel that reduces blood flow in the lumen, which may cause ischemic cardiovascular complications. On the surface of atherosclerotic plaques associated with severe stenosis, shear stress imposes a risk of thrombosis and sudden occlusion (3). Therefore, a stenotic plaque may be a vulnerable plaque regardless of presence or absence of ischemia (3). Moreover, a stenotic plaque may indicate the presence of many nonstenotic or less-stenotic plaques that could be vulnerable to rupture and thrombosis (56,57).

MR angiography of the carotid arteries has gone through a long evolutionary period to become a routine imaging modality for evaluation of stenosis at many centers (58,59). In carotid arteries, the ability of MR angiography to demonstrate less than 70% versus 70%–99% stenosis is much better than that of duplex US (60). Also, MR angiography is a sensitive and specific test when digital subtraction angiography is used as the reference standard (61).

However, noninvasive imaging of the coronary arteries is a formidable task: The small diameter of the coronary arteries (approximately 2–4 mm), their tortuous course, their close anatomic relationship to the coronary veins and cardiac chambers, and, finally, their continuous rapid motion due to cardiac contractions and respiratory excursions create obstacles that are difficult to overcome. Kim et al (60) used a free-breathing, navigator-gated, three-dimensional MR technique to depict the coronary arteries and help detect coronary stenoses in a series of 109 patients (Fig 5). In segments that could be evaluated, 78 of 94 stenoses of more than 50% were detected by using MR angiog-
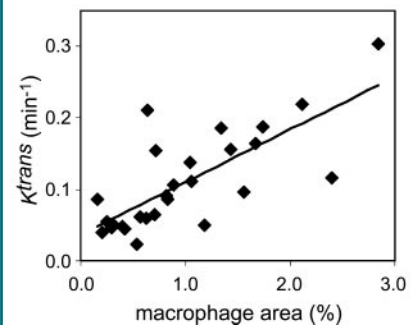
Figure 4: Scatterplot demonstrates correlation between dynamic contrast-enhanced MR imaging and corresponding histologic findings. There is a highly significant association between K^{trans} as measured on MR images and degree of macrophage infiltration of the plaque on histologic specimens (fractional macrophage area) (Pearson $R = 0.75$, $P < .001$). (Reprinted, with permission, from reference 48.)

raphy, with conventional coronary angiography as the reference standard. In a separate analysis, the authors calculated a sensitivity of 100% for the identification of either left main coronary artery disease or three-vessel disease, conditions in which revascularization is of particular therapeutic value. However, current spatial (approximately $1 \times 1 \times 2$-mm) and temporal (approximately 60–125-msec) resolutions permit imaging only of the proximal two-thirds of the coronary arteries, exclusive of the major side branches (62). Though coronary MR angiography is promising, further development is needed before it can enter routine clinical use (62).

Recently, alternative acquisition techniques, such as steady-state free precession (64), have been proposed (63) that establish different contrast behavior and use different k-space acquisition schemes, such as spiral (65) or radial (also known as projection-reconstruction) (66) readout patterns. Furthermore, a whole-heart steady-state free-precession coronary MR angiography technique has been proposed (63) that improves visible vessel length and facilitates high-quality coronary MR angiography of the complete coronary tree in a single measurement. These newer sequences are reported to provide several advantages over the free-

Radiology

breathing T2-prepared segmented gradient-recalled-echo sequence (67,68). The advantages include increases in signal-to-noise ratio, contrast-to-noise ratio, vessel sharpness, and coverage of vessel length, as well as reduction in acquisition time.

Traditionally, the degree of stenosis is assessed on a projection angiogram by using the North American Symptomatic Carotid Endarterectomy Trial (NASCET) criteria, the European Carotid Surgery Trial (ECST) criteria, the common carotid method, or the so-called eyeballing method (69). While it has been demonstrated that the degree of ipsilateral carotid stenosis, as measured with the techniques used in the ECST and NASCET, clearly predict stroke risk (70,71), all of these techniques have sizable disagreements among repeated measurements for some vessels (68).
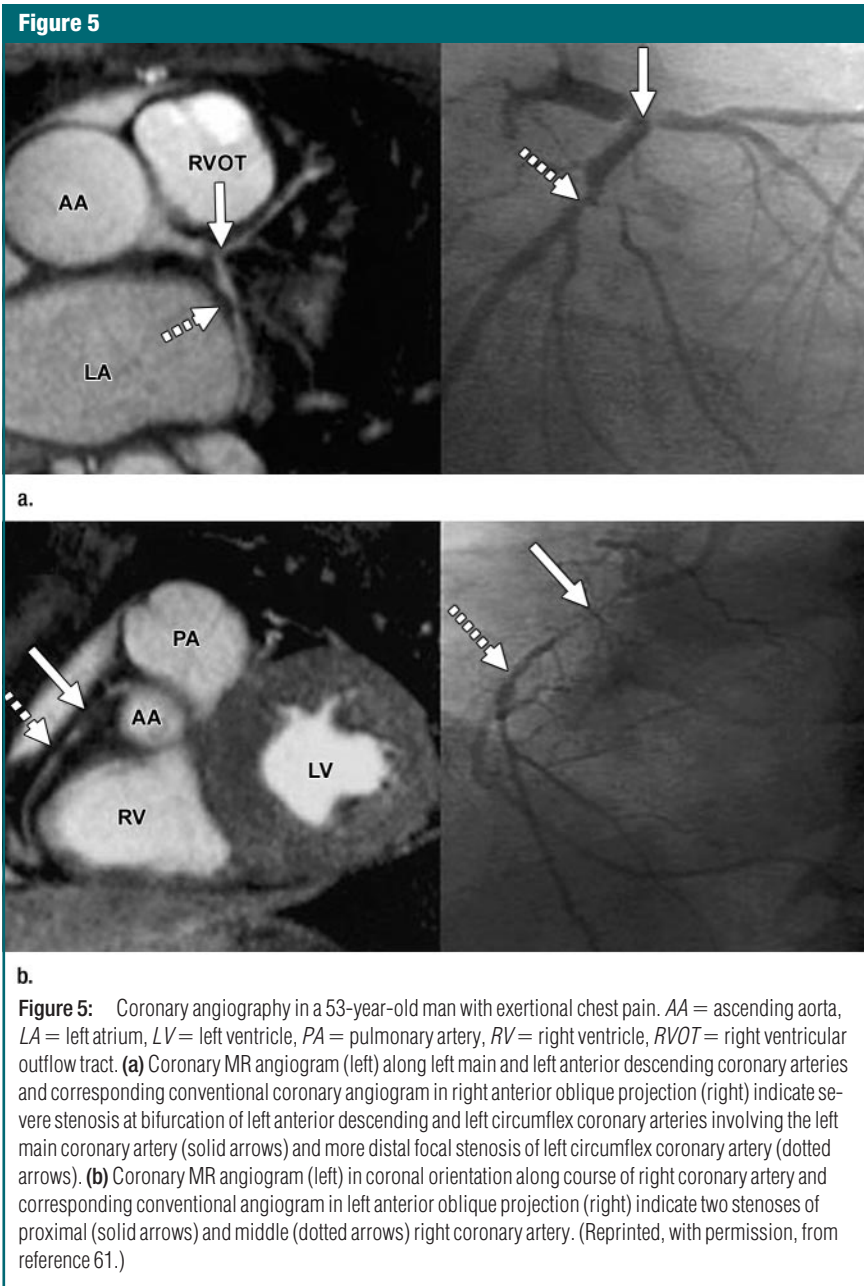
For evaluation of the degree of stenosis on projection angiograms, the minimum luminal diameter at a target site is determined. The projection image should be generated at an angle that allows measurement of the minimum luminal diameter; this dimension may not be measurable in cases of eccentric stenosis with images generated at suboptimal angles (72). In contrast, on cross-sectional images the minimum luminal diameter can be measured accurately without difficulty (72,73), and some investigators state that a reduction in cross-sectional area correlates better with the hemodynamic effect of stenosis than does a reduction in diameter (74). In the future, new computerized carotid stenosis measurement systems that measure the stenosis by using transverse MR angiographic images (75,76) have the potential to further reduce variability.

Minor Criteria

Superficial Calcified Nodule

The consensus documents (3,4) describe a type of plaque that has a calcified nodule within or very close to the fibrous cap, and this structure protrudes through and can rupture the cap (3). It has been shown in coronary arteries that the presence of calcified nodules is not necessarily associated with severe coronary calcification and a high calcium score (17).

In vivo MR imaging is able to depict overall plaque calcification with good sensitivity and specificity (9). Furthermore, a strong correlation between MR and histologic area measurements has been achieved ($r = 0.74$, $P < .001$) (9). However, juxtaluminal calcification can be more difficult to identify than calcification that is deeper within the plaque, because juxtaluminal calcification appears as a hypointense signal on TOF and T1-, intermediate-, and T2-weighted images and is not distinguishable from the lumen on black-blood T1-, intermediate-, and T2-weighted images. However, the addition of bright-blood TOF imaging facilitates identification of juxtaluminal calcification, in that it is

Figure 5

Figure 5: Coronary angiography in a 53-year-old man with exertional chest pain. *AA* = ascending aorta, *LA* = left atrium, *LV* = left ventricle, *PA* = pulmonary artery, *RV* = right ventricle, *RVOT* = right ventricular outflow tract. **(a)** Coronary MR angiogram (left) along left main and left anterior descending coronary arteries and corresponding conventional coronary angiogram in right anterior oblique projection (right) indicate severe stenosis at bifurcation of left anterior descending and left circumflex coronary arteries involving the left main coronary artery (solid arrows) and more distal focal stenosis of left circumflex coronary artery (dotted arrows). **(b)** Coronary MR angiogram (left) in coronal orientation along course of right coronary artery and corresponding conventional angiogram in left anterior oblique projection (right) indicate two stenoses of proximal (solid arrows) and middle (dotted arrows) right coronary artery. (Reprinted, with permission, from reference 61.)

clearly distinguishable from the bright lumen on TOF images. Recent reports (20,38) have provided preliminary evidence that the combined use of black-blood and bright-blood images makes feasible the detection of calcified nodules and/or juxtaluminal calcification in the carotid arteries (Fig 6).

Glistening Yellow Plaques at Angioscopy

Yellow plaques, particularly glistening ones, may indicate a large lipid-necrotic core and a thin fibrous cap, suggesting a high risk of rupture. However, because plaques in different stages can be yellow and not all lipid-laden plaques are destined to rupture or undergo thrombosis, this criterion may lack sufficient specificity (77,78). Furthermore, this criterion is determined solely on the basis of angioscopic observations. Angioscopy is an intravascular imaging method that achieves high spatial resolution. However, the information is limited to the luminal surface, the technique is invasive and highly operator dependent, and it is currently not approved by the Food and Drug Administration for use in the United States. Obviously, MR images cannot depict the color of the plaque's surface. However, as mentioned earlier in the section Thin Cap with Large Lipid-Necrotic Core, invivo MR imaging is able to depict lipid-necrotic cores and the status of the fibrous cap, both features of angioscopically glistening yellow plaques.

Intraplaque Hemorrhage

Extravasation of red blood cells or iron accumulation in plaque may represent plaque instability and promote plaque progression (3,79). The mechanism that results in intraplaque hemorrhages is not completely understood: Constantinides (80) and others (81) have suggested that hemorrhage into a plaque occurs from cracks or fissures that originate at the luminal surface, while Paterson (82) has proposed that intraplaque hemorrhage is secondary to rupture of the vasa vasorum, a common feature of advanced lesions with plaque rupture and luminal thrombi.

In vivo MR imaging is able to depict carotid intraplaque hemorrhage (Fig

Figure 6
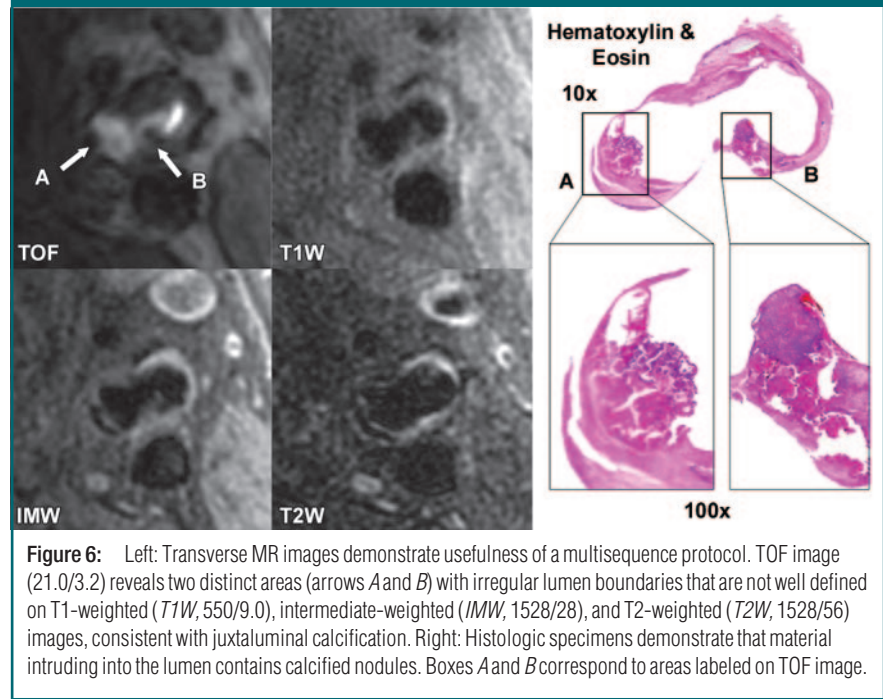
Figure 6: Left: Transverse MR images demonstrate usefulness of a multisequence protocol. TOF image (21.0/3.2) reveals two distinct areas (arrows *A* and *B*) with irregular lumen boundaries that are not well defined on T1-weighted (*T1W*, 550/9.0), intermediate-weighted (*IMW*, 1528/28), and T2-weighted (*T2W*, 1528/56) images, consistent with juxtaluminal calcification. Right: Histologic specimens demonstrate that material intruding into the lumen contains calcified nodules. Boxes *A* and *B* correspond to areas labeled on TOF image.

3a) with good sensitivity and moderate to good specificity (13,20,83–85). Furthermore it has been shown that MR imaging can help differentiate between hemorrhages of different ages (83) with the use of modified criteria for cerebral hemorrhage. Moody et al (84) showed that T1-weighted images of the carotid arteries can be used to accurately identify histologically confirmed complicated plaque with hemorrhage or thrombus.

Though intraplaque hemorrhage is listed as a minor criterion, recent articles (79,86,87) suggest a greater role of hemorrhage in plaque destabilization than was previously thought. Results of a study of 24 patients (79) who had died suddenly of coronary causes suggested that hemorrhage contributed to the deposition of free cholesterol, infiltration by macrophages, and enlargement of the necrotic core, thereby representing a potent atherogenic stimulus. Consistent with this notion, a recent prospective longitudinal MR investigation (87) of 31 patients showed that hemorrhage into a carotid plaque accelerated plaque progression in a period of 18 months. The percent change in wall volume (6.8% vs −0.15%, $P = .009$) and

lipid-necrotic core volume (28.4% vs −5.2%, $P = .001$) was significantly higher in the hemorrhage group than in the control group (Fig 7). Further, patients with intraplaque hemorrhage at baseline showed a far greater susceptibility to repeat plaque hemorrhages (87). Therefore, intraplaque hemorrhage may represent a critical transition, promoting the conversion of a stable to an unstable plaque phenotype (86).

Endothelial Dysfunction

Studies have shown that endothelial dysfunction is associated with coronary heart disease and stroke (88,89). Furthermore, vulnerable plaques with active inflammation and oxidative stress are likely to be associated with impaired endothelial function (3).

Although in vivo MR imaging is not able to depict the endothelium directly, MR and a number of other imaging modalities can be used to measure arterial stiffness noninvasively (90). Arterial stiffness and endothelial dysfunction commonly coexist in patients at increased risk of cardiovascular disease (90), for example in patients with diabe-

tes (91) and in smokers (92). Indeed, some studies in children have directly related increased stiffness with impaired endothelial function (93,94).

Although MR imaging can help assess various stiffness parameters such as vascular distensibility, flow measurements, and pulse wave velocity by using true fast imaging with steady-state free precession (95) and gradient-recalled-echo pulse sequences with a velocity-encoding gradient for phase-contrast MR (96,97), only a few such investigations have been performed in this field (90). This is due to the large number of other imaging modalities, such as Doppler US or applanation tonometry, which also allow evaluation of arterial stiffness (90). However, a recent study showed that MR imaging offers insights not otherwise possible (90) with regard to describing an age-related increase in pulse wave velocity in the proximal aorta relative to that in the distal aorta (97). In another MR investigation (95) in which central vascular distensibility was assessed, pulse wave velocity and flow-mediated dilatation showed global impairment of brachial, carotid, and aortic vascular function in young smokers.

Another indirect MR measure of the endothelial function is to measure the transfer constant K^{trans} by using dy-namic contrast-enhanced MR imaging (48). This parameter quantifies the increased vascularity, permeability, and extracellular water content typically associated with the inflammatory response.

Outward (Positive) Remodeling

Many nonstenotic lesions undergo "expansive," "positive," or "outward" remodeling: namely, compensatory enlargement that permits growth in overall plaque size without reduction in luminal area. Several authors (98,99) have suggested that such remodeling is a potential surrogate marker of plaque vulnerability. MR imaging is ideally suited for serial and noninvasive assessment of arterial remodeling, because MR provides information about the lumen and arterial wall simultaneously.

Clinical trials of MR imaging to examine the results of statin therapy on plaque progression or regression have demonstrated a greater effect on vessel wall area than on changes in lumen dimensions, which suggests a remodeling process on the vessel wall. Corti et al (100) performed serial carotid and aortic MR imaging in patients treated with simvastatin and found that vessel wall area and vessel wall thickness decreased by 18% and 19%, respectively,

in carotid lesions and by 16% and 16%, respectively, in thoracic lesions at 24 months (Fig 8). Lumen area increased by only 5% after 24 months of statin therapy. Recently, Yonemura et al (101) reported the results of a prospective, randomized, open-label trial to elucidate the effects on atherosclerotic plaques in the thoracic aorta of atorvastatin dosages of 20 mg/d versus 5 mg/d. Their results indicated that the 20 mg/d dose reduced maximal vessel wall thickness and vessel wall area of thoracic aortic plaques (−12% and −18%, respectively; $P < .001$), whereas 5 mg/d did not (+1% and +4%, respectively). Lumen area increased 5% in the high-dose group and 0% in the low-dose group.

In a study that included six healthy subjects and six subjects with nonsignificant coronary artery disease (10%–50% diameter reduction on conventional angiogram), Kim et al (102) introduced a noninvasive MR imaging method to demonstrate expansive remodeling in coronary arteries. Free-breathing three-dimensional black-blood coronary MR imaging with isotropic resolution depicted an increased coronary vessel wall thickness with preservation of lumen size in patients with nonsignificant coronary artery disease, consistent with expansive arterial remodeling. A recent study (103) in 15 volunteers demonstrated the feasibility of coronary wall MR imaging with free-breathing and breath-hold two-dimensional black-blood turbo spin-echo sequences at 3 T. Although measurements of coronary wall thickness and area and lumen diameter and area were consistent with previous MR measurements at 1.5 T, the authors concluded that further improvement in resolution and image quality is required to enable detection and characterization of coronary plaques (103).

Summary, Clinical Perspectives, and Conclusion

Noninvasive MR imaging has the potential to help identify, directly or indirectly, most of the consensus criteria for the identification of vulnerable plaque in larger vessels by using a vari-
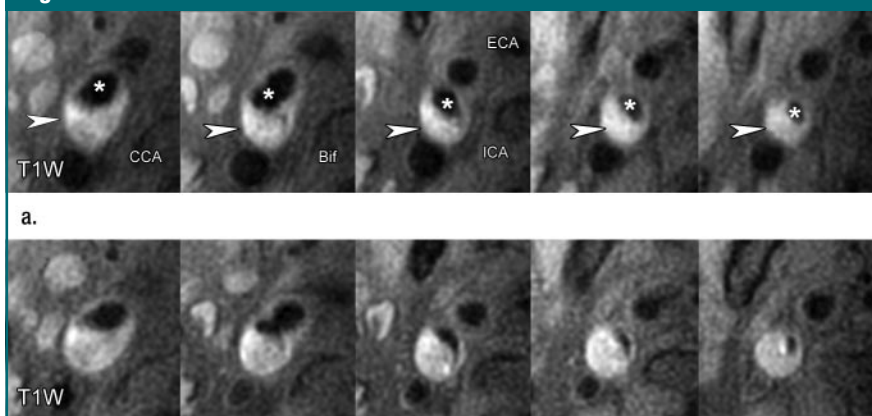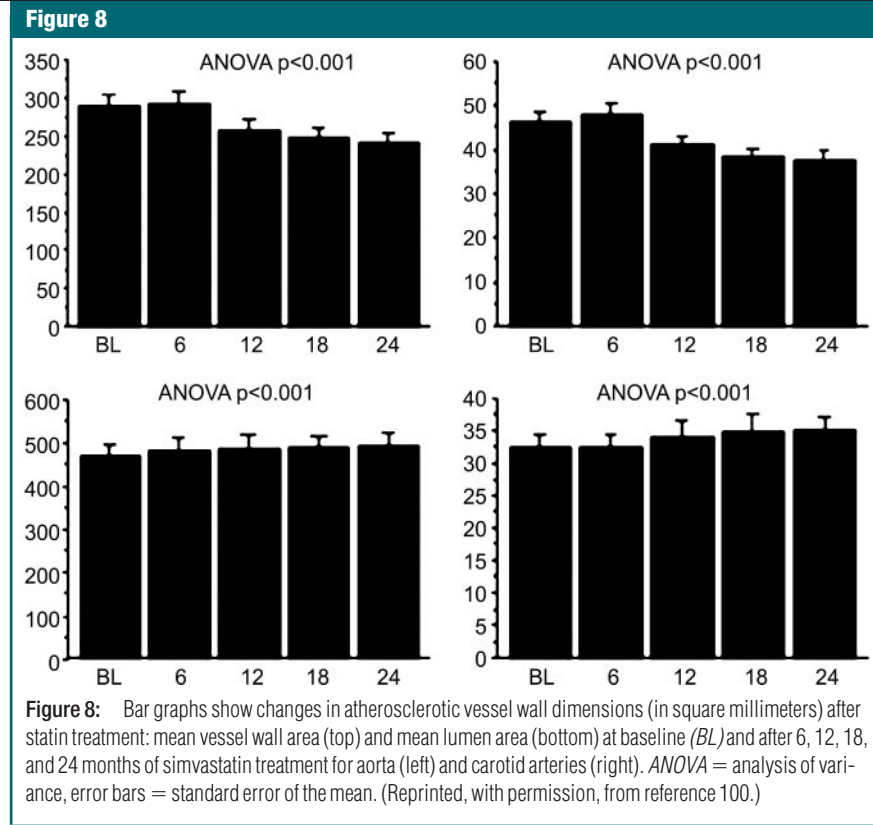

Figure 7: Representative transverse T1-weighted MR images (800/9.3) of the progression of atherosclerosis with intraplaque hemorrhage. Right carotid artery was imaged **(a)** at baseline and **(b)** 18 months later. Lumen area (∗) decreased and wall area (arrowheads) increased in each section on **b.** *Bif* = bifurcation, *CCA* = common carotid artery, *ECA* = external carotid artery, *ICA* = internal carotid artery. (Reprinted, with permission, from reference 87.)

Radiology

ety of proposed image-acquisition and contrast enhancement techniques (see Table 2). Thus far, there is not a single MR technique that can be used to assess all the vulnerable plaque criteria, and it remains to be seen which imaging approach, if any, will be commonly used in clinical practice. While some of the proposed image acquisition techniques rely on one (11) or two (26,36,85,101) MR sequences, others are based on the acquisition of multiple contrast-weighted images (9,10,104).

The number and types of sequences used depend on which plaque characteristics are to be studied. For instance, rapid assessment of overall plaque burden is feasible by using one or two MR sequences (100,105). To evaluate plaque composition and morphology in one imaging session, however, most studies rely on multiple MR sequences (9,10,104). Black-blood T1-, intermediate-, and T2-weighted images with fat (8) and flow suppression (106) enable visualization of the full vessel wall and are needed to characterize the major plaque components, such as a lipid-necrotic core, calcification, and a loose fibrous matrix (9). Bright-blood TOF images are needed for evaluation of the status of the fibrous cap (15,28) and identification of calcified nodules (see Fig 6) (20). Other sequences, such as contrast-enhanced T1-weighted images (22,27) and dynamic contrast-enhanced two-dimensional spoiled gradient-recalled-echo images (48) are useful for quantifying the size of the lipid-necrotic core (22) and evaluating plaque inflammation (47,48). Furthermore, the use of sophisticated contrast agents, such as ultrasmall superparamagnetic iron oxides (53,54) and fibrin-targeted (41,42) and $\alpha v\beta 3$-integrin–targeted (55) nanoparticles offers the promise of in vivo targeted imaging of the plaque (7).

The ability to distinguish stable from vulnerable plaques may ultimately permit identification of patients with low versus those with high risk of cardiovascular complications. Furthermore, in vivo MR imaging has potential as a tool for screening for atherosclerosis and for serial monitoring of disease progression or regression. It is important to note

Figure 8

Figure 8: Bar graphs show changes in atherosclerotic vessel wall dimensions (in square millimeters) after statin treatment: mean vessel wall area (top) and mean lumen area (bottom) at baseline *(BL)* and after 6, 12, 18, and 24 months of simvastatin treatment for aorta (left) and carotid arteries (right). *ANOVA* = analysis of variance, error bars = standard error of the mean. (Reprinted, with permission, from reference 100.)

that the consensus document (3,4) criteria that define the vulnerable plaque are based on histologic studies of culprit plaques. Histologic examination can only capture information regarding the plaque from a single time point. Thus, little is known about the evolution of vulnerable plaques, and noninvasive serial MR imaging of such plaques can, therefore, provide useful insights into their natural history and might help to identify plaques that are on a trajectory of evolution toward a vulnerable state.

In a recent prospective in vivo MR imaging study (107) that used T1-, T2-, and intermediate-weighted images and TOF images, the authors investigated the association between carotid plaque characteristics and subsequent ischemic cerebrovascular events in 154 subjects who initially had an asymptomatic 50%–79% carotid stenosis seen at duplex US. During a mean follow-up of 38.2 months, 12 carotid cerebrovascular events occurred. Cox regression analysis indicated that plaques with intraplaque hemorrhage (hazard ratio:

4.7; 95% confidence interval: 1.6, 14.0; $P = .004$), larger mean intraplaque hemorrhage area (hazard ratio for 10-mm^2 increase: 2.4; 95% confidence interval: 1.4, 4.1; $P = .008$), thin or ruptured fibrous cap (hazard ratio: 9.4; 95% confidence interval: 2.1, 42.1; $P < .001$), larger maximum percentage lipid-rich–to-necrotic core ratio (hazard ratio for 10% increase: 1.4; 95% confidence interval: 1.1, 1.9; $P = .01$), and maximum wall thickness (hazard ratio for 1-mm increase: 1.6; 95% confidence interval, 1.1, 2.1; $P = .007$) were associated with the cerebrovascular events.

Although initial findings of this prospective study (107) were promising, several challenges remain. Most of the in vivo MR studies in humans cited in this article were based on analysis of data from relatively large human vessels, such as the carotid arteries. To achieve similar results in the much smaller coronary arteries, substantial advances in temporal and spatial resolution are necessary. This may be accomplished with improvements in pulse se-

Radiology

quence design and MR hardware (eg, higher field strength, new coil designs). Therefore, prospective studies in large populations are needed to determine the predictive value of MR-based assessment of vulnerable plaque features for subsequent ischemic events.

References

1. World Health Organization. World Health Statistics 2005. http://www.who.int/healthinfo/statistics/whsatsdownloads/en/index.html. Published 2005. Accessed April 18, 2007.

2. Weinberger J. Diagnosis and prevention of atherosclerotic cerebral infarction. CNS Spectr 2005;10:553–564.

3. Naghavi M, Libby P, Falk E, et al. From vulnerable plaque to vulnerable patient: a call for new definitions and risk assessment strategies—part I. Circulation 2003;108:1664–1672.

4. Naghavi M, Libby P, Falk E, et al. From vulnerable plaque to vulnerable patient: a call for new definitions and risk assessment strategies—part II. Circulation 2003;108:1772–1778.

5. Mistretta CA. Relative characteristics of MR angiography and competing vascular imaging modalities. J Magn Reson Imaging 1993;3:685–698.

6. Saam T, Kerwin WS, Yuan C. Vascular imaging. In: Wnek GE, Bowlin GL, eds. Encyclopedia of biomaterials and biomedical engineering. New York, NY: Dekker, 2004.

7. Choudhury RP, Fuster V, Badimon JJ, Fisher EA, Fayad ZA. MRI and characterization of atherosclerotic plaque: emerging applications and molecular imaging. Arterioscler Thromb Vasc Biol 2002;22:1065–1074.

8. Yuan C, Mitsumori LM, Beach KW, Maravilla KR. Carotid atherosclerotic plaque: noninvasive MR characterization and identification of vulnerable lesions. Radiology 2001;221:285–299.

9. Saam T, Ferguson MS, Yarnykh VL, et al. Quantitative evaluation of carotid plaque composition by in vivo MRI. Arterioscler Thromb Vasc Biol 2005;25:234–239.

10. Clarke SE, Hammond RR, Mitchell JR, Rutt BK. Quantitative assessment of carotid plaque composition using multicontrast MRI and registered histology. Magn Reson Med 2003;50:1199–1208.

11. Serfaty JM, Chaabane L, Tabib A, Chevallier JM, Briguet A, Douek PC. Atherosclerotic plaques: classification and characterization with T2-weighted high-spatial-resolution MR imaging—an in vitro study. Radiology 2001;219:403–410.

12. Shinnar M, Fallon JT, Wehrli S, et al. The diagnostic accuracy of ex vivo MRI for human atherosclerotic plaque characterization. Arterioscler Thromb Vasc Biol 1999;19:2756–2761.

13. Toussaint JF, LaMuraglia GM, Southern JF, Fuster V, Kantor HL. Magnetic resonance images lipid, fibrous, calcified, hemorrhagic, and thrombotic components of human atherosclerosis in vivo. Circulation 1996;94:932–938.

14. Cai JM, Hatsukami TS, Ferguson MS, Small R, Polissar NL, Yuan C. Classification of human carotid atherosclerotic lesions with in vivo multicontrast magnetic resonance imaging. Circulation 2002;106:1368–1373.

15. Hatsukami TS, Ross R, Polissar NL, Yuan C. Visualization of fibrous cap thickness and rupture in human atherosclerotic carotid plaque in vivo with high-resolution magnetic resonance imaging. Circulation 2000;102:959–964.

16. Yuan C, Kerwin WS. MRI of atherosclerosis. J Magn Reson Imaging 2004;19:710–719.

17. Virmani R, Kolodgie FD, Burke AP, Farb A, Schwartz SM. Lessons from sudden coronary death: a comprehensive morphological classification scheme for atherosclerotic lesions. Arterioscler Thromb Vasc Biol 2000;20:1262–1275.

18. Stary HC, Chandler AB, Dinsmore RE, et al. A definition of advanced types of atherosclerotic lesions and a histological classification of atherosclerosis: a report from the Committee on Vascular Lesions of the Council on Arteriosclerosis, American Heart Association. Circulation 1995;92:1355–1374.

19. Burke AP, Weber DK, Kolodgie FD, Farb A, Taylor AJ, Virmani R. Pathophysiology of calcium deposition in coronary arteries. Herz 2001;26:239–244.

20. Yuan C, Mitsumori LM, Ferguson MS, et al. In vivo accuracy of multispectral magnetic resonance imaging for identifying lipid-rich necrotic cores and intraplaque hemorrhage in advanced human carotid plaques. Circulation 2001;104:2051–2056.

21. Yuan C, Kerwin WS, Ferguson MS, et al. Contrast-enhanced high resolution MRI for atherosclerotic carotid artery tissue characterization. J Magn Reson Imaging 2002;15:62–67.

22. Cai J, Hatsukami TS, Ferguson MS, et al. In vivo quantitative measurement of intact fibrous cap and lipid-rich necrotic core size in atherosclerotic carotid plaque: comparison of high-resolution, contrast-enhanced magnetic resonance imaging and histology. Circulation 2005;112:3437–3444.

23. Parker DL, Yuan C, Blatter DD. MR angiography by multiple thin slab 3D acquisition. Magn Reson Med 1991;17:434–451.

24. Mitsumori LM, Hatsukami TS, Ferguson MS, Kerwin WS, Cai J, Yuan C. In vivo accuracy of multisequence MR imaging for identifying unstable fibrous caps in advanced human carotid plaques. J Magn Reson Imaging 2003;17:410–420.

25. Trivedi RA, King-Im J, Graves MJ, et al. Multi-sequence in vivo MRI can quantify fibrous cap and lipid core components in human carotid atherosclerotic plaques. Eur J Vasc Endovasc Surg 2004;28:207–213.

26. Kramer CM, Cerilli LA, Hagspiel K, DiMaria JM, Epstein FH, Kern JA. Magnetic resonance imaging identifies the fibrous cap in atherosclerotic abdominal aortic aneurysm. Circulation 2004;109:1016–1021.

27. Wasserman BA, Smith WI, Trout HH III, Cannon RO 3rd, Balaban RS, Arai AE. Carotid artery atherosclerosis: in vivo morphologic characterization with gadolinium-enhanced double-oblique MR imaging—initial results. Radiology 2002;223:566–573.

28. Yuan C, Zhang SX, Polissar NL, et al. Identification of fibrous cap rupture with magnetic resonance imaging is highly associated with recent transient ischemic attack or stroke. Circulation 2002;105:181–185.

29. Falk E, Shah PK, Fuster V. Coronary plaque disruption. Circulation 1995;92:657–671.

30. Wentzel JJ, Aguiar SH, Fayad ZA. Vascular MRI in the diagnosis and therapy of the high risk atherosclerotic plaque. J Interv Cardiol 2003;16:129–142.

31. Toussaint JF, Southern JF, Fuster V, Kantor HL. Water diffusion properties of human atherosclerosis and thrombosis measured by pulse field gradient nuclear magnetic resonance. Arterioscler Thromb Vasc Biol 1997;17:542–546.

32. Bradley WG Jr. MR appearance of hemorrhage in the brain. Radiology 1993;189:15–26.

33. Chu K, Kang DW, Yoon BW, Roh JK. Diffusion-weighted magnetic resonance in cerebral venous thrombosis. Arch Neurol 2001;58:1569–1576.

34. Yoshikawa T, Abe O, Tsuchiya K, et al. Diffusion-weighted magnetic resonance imaging of dural sinus thrombosis. Neuroradiology 2002;44:481–488.

35. Taber KH, Hayman LA, Herrick RC, Kirk-

patrick JB. Importance of clot structure in gradient-echo magnetic resonance imaging of hematoma. J Magn Reson Imaging 1996; 6:878–883.

36. Corti R, Osende JI, Fayad ZA, et al. In vivo noninvasive detection and age definition of arterial thrombus by MRI. J Am Coll Cardiol 2002;39:1366–1373.

37. Paydarfar D, Krieger D, Dib N, et al. In vivo magnetic resonance imaging and surgical histopathology of intracardiac masses: distinct features of subacute thrombi. Cardiology 2001;95:40–47.

38. Kampschulte A, Ferguson MS, Kerwin WS, et al. Differentiation of intraplaque versus juxtaluminal hemorrhage/thrombus in advanced human carotid atherosclerotic lesions by in vivo magnetic resonance imaging. Circulation 2004;110:3239–3244.

39. Saam T, Cai J, Ma L, et al. Comparison of symptomatic and asymptomatic atherosclerotic carotid plaque features with in vivo MR imaging. Radiology 2006;240(2):464–472.

40. Yu X, Song SK, Chen J, et al. High-resolution MRI characterization of human thrombus using a novel fibrin-targeted paramagnetic nanoparticle contrast agent. Magn Reson Med 2000;44:867–872.

41. Flacke S, Fischer S, Scott MJ, et al. Novel MRI contrast agent for molecular imaging of fibrin: implications for detecting vulnerable plaques. Circulation 2001;104:1280–1285.

42. Botnar RM, Perez AS, Witte S, et al. In vivo molecular imaging of acute and subacute thrombosis using a fibrin-binding magnetic resonance imaging contrast agent. Circulation 2004;109:2023–2029.

43. Botnar RM, Buecker A, Wiethoff AJ, et al. In vivo magnetic resonance imaging of coronary thrombosis using a fibrin-binding molecular magnetic resonance contrast agent. Circulation 2004;110:1463–1466.

44. Spuentrup E, Buecker A, Katoh M, et al. Molecular magnetic resonance imaging of coronary thrombosis and pulmonary emboli with a novel fibrin-targeted contrast agent. Circulation 2005;111:1377–1382.

45. Hansson GK. Inflammation, atherosclerosis, and coronary artery disease. N Engl J Med 2005;352:1685–1695.

46. Bassiouny HS, Sakaguchi Y, Mikucki SA, et al. Juxtalumenal location of plaque necrosis and neoformation in symptomatic carotid stenosis. J Vasc Surg 1997;26:585–594.

47. Kerwin W, Hooker A, Spilker M, et al. Quantitative magnetic resonance imaging analysis of neovasculature volume in carotid atherosclerotic plaque. Circulation 2003;107:851–856.

48. Kerwin WS, O'Brien KD, Ferguson MS, Polissar N, Hatsukami TS, Yuan C. Inflammation in carotid atherosclerotic plaque: a dynamic contrast-enhanced MR imaging study. Radiology 2006;241(2):459–468.

49. Lin W, Abendschein DR, Haacke EM. Contrast-enhanced magnetic resonance angiography of carotid arterial wall in pigs. J Magn Reson Imaging 1997;7:183–190.

50. Aoki S, Aoki K, Ohsawa S, Nakajima H, Kumagai H, Araki T. Dynamic MR imaging of the carotid wall. J Magn Reson Imaging 1999;9:420–427.

51. McCarthy MJ, Loftus IM, Thompson MM, et al. Angiogenesis and the atherosclerotic carotid plaque: an association between symptomatology and plaque morphology. J Vasc Surg 1999;30:261–268.

52. Schmitz SA, Taupitz M, Wagner S, Wolf KJ, Beyersdorff D, Hamm B. Magnetic resonance imaging of atherosclerotic plaques using superparamagnetic iron oxide particles. J Magn Reson Imaging 2001;14:355–361.

53. Ruehm SG, Corot C, Vogt P, Kolb S, Debatin JF. Magnetic resonance imaging of atherosclerotic plaque with ultrasmall superparamagnetic particles of iron oxide in hyperlipidemic rabbits. Circulation 2001;103: 415–422.

54. Kooi ME, Cappendijk VC, Cleutjens KB, et al. Accumulation of ultrasmall superparamagnetic particles of iron oxide in human atherosclerotic plaques can be detected by in vivo magnetic resonance imaging. Circulation 2003;107:2453–2458.

55. Winter PM, Morawski AM, Caruthers SD, et al. Molecular imaging of angiogenesis in early-stage atherosclerosis with alpha(v)beta3-integrin-targeted nanoparticles. Circulation 2003;108:2270-2274.

56. Goldstein JA, Demetriou D, Grines CL, Pica M, Shoukfeh M, O'Neill WW. Multiple complex coronary plaques in patients with acute myocardial infarction. N Engl J Med 2000;343:915–922.

57. Asakura M, Ueda Y, Yamaguchi O, et al. Extensive development of vulnerable plaques as a pan-coronary process in patients with myocardial infarction: an angioscopic study. J Am Coll Cardiol 2001;37: 1284–1288.

58. Rapp JH, Saloner D. Current status of carotid imaging by MRA. Cardiovasc Surg 2003;11:445–447.

59. Huston J III, Fain SB, Wald JT, et al. Carotid artery: elliptic centric contrast-enhanced MR angiography compared with conventional angiography. Radiology 2001; 218:138–143.

60. Kim WY, Danias PG, Stuber M, et al. Coronary magnetic resonance angiography for the detection of coronary stenoses. N Engl J Med 2001;345:1863–1869.

61. Nederkoorn PJ, van der Graff Y, Hunink MG. Duplex ultrasound and magnetic resonance angiography compared with digital subtraction angiography in carotid artery stenosis: a systematic review. Stroke 2003; 34:1324–1332.

62. Ropers D, Regenfus M, Wasmeier G, Achenbach S. Non-interventional cardiac diagnostics: computed tomography, magnetic resonance and real-time three-dimensional echocardiography—techniques and clinical applications. Minerva Cardioangiol 2004;52:407–417.

63. Weber OM, Pujadas S, Martin AJ, Higgins CB. Free-breathing, three-dimensional coronary artery magnetic resonance angiography: comparison of sequences. J Magn Reson Imaging 2004;20:395–402.

64. Deshpande VS, Shea SM, Laub G, Simonetti OP, Finn JP, Li D. 3D magnetization-prepared true-FISP: a new technique for imaging coronary arteries. Magn Reson Med 2001;46:494–502.

65. Bornert P, Stuber M, Botnar RM, et al. Direct comparison of 3D spiral vs. Cartesian gradient-echo coronary magnetic resonance angiography. Magn Reson Med 2001; 46:789–794.

66. Katoh M, Stuber M, Buecker A, Gunther RW, Spuentrup E. Spin-labeling coronary MR angiography with steady-state free precession and radial k-space sampling: initial results in healthy volunteers. Radiology 2005;236(3):1047–1052.

67. Botnar RM, Stuber M, Danias PG, Kissinger KV, Manning WJ. Improved coronary artery definition with T2-weighted, free-breathing, three-dimensional coronary MRA. Circulation 1999;99:3139–3148.

68. Stuber M, Botnar RM, Danias PG, et al. Double-oblique free-breathing high resolution three-dimensional coronary magnetic resonance angiography. J Am Coll Cardiol 1999;34:524–531.

69. Young GR, Humphrey PR, Nixon TE, Smith ET. Variability in measurement of extracranial internal carotid artery stenosis as displayed by both digital subtraction and magnetic resonance angiography: an assessment of three caliper techniques and visual impression of stenosis. Stroke 1996;27:467–473.

70. North American Symptomatic Carotid Endarterectomy Trial. Methods, patient char-

acteristics, and progress. Stroke 1991;22: 711–720.

71. European Carotid Surgery Trialists' Collaborative Group. MRC European Carotid Surgery Trial: interim results for symptomatic patients with severe (70–99%) or with mild (0–29%) carotid stenosis. Lancet 1991; 337:1235–1243.

72. Ota H, Takase K, Rikimaru H, et al. Quantitative vascular measurements in arterial occlusive disease. RadioGraphics 2005;25: 1141–1158.

73. Morasch MD, Gurjala AN, Washington E, et al. Cross-sectional magnetic resonance angiography is accurate in predicting degree of carotid stenosis. Ann Vasc Surg 2002;16:266–272.

74. Dodds SR. The haemodynamics of asymmetric stenoses. Eur J Vasc Endovasc Surg 2002;24:332–337.

75. Kim DY, Park JW. Computerized quantification of carotid artery stenosis using MRA axial images. Magn Reson Imaging 2004;22: 353–359.

76. van Bemmel CM, Viergever MA, Niessen WJ. Semiautomatic segmentation and stenosis quantification of 3D contrast-enhanced MR angiograms of the internal carotid artery. Magn Reson Med 2004;51: 753–760.

77. Kodama K, Asakura M, Ueda Y, Yamaguchi O, Hirayama A. The role of plaque rupture in the development of acute coronary syndrome evaluated by the coronary angioscope. Intern Med 2000;39:333–335.

78. Takano M, Mizuno K, Okamatsu K, Yokoyama S, Ohba T, Sakai S. Mechanical and structural characteristics of vulnerable plaques: analysis by coronary angioscopy and intravascular ultrasound. J Am Coll Cardiol 2001;38:99–104.

79. Kolodgie FD, Gold HK, Burke AP, et al. Intraplaque hemorrhage and progression of coronary atheroma. N Engl J Med 2003; 349:2316–2325.

80. Constantinides P. Plaque fissuring in human coronary thrombosis. J Atheroscler Res 1966;6:1–17.

81. Davies MJ, Thomas AC. Plaque fissuring: the cause of acute myocardial infarction, sudden ischaemic death, and crescendo angina. Br Heart J 1985;53:363–373.

82. Paterson JC. Capillary rupture with intimal hemorrhage as a causative factor in coronary thrombosis. Arch Pathol 1938;25: 474–487.

83. Chu B, Kampschulte A, Ferguson MS, et al. Hemorrhage in the atherosclerotic carotid plaque: a high-resolution MRI study. Stroke 2004;35:1079–1084.

84. Moody AR, Murphy RE, Morgan PS, et al. Characterization of complicated carotid plaque with magnetic resonance direct thrombus imaging in patients with cerebral ischemia. Circulation 2003;107:3047–3052.

85. Cappendijk VC, Cleutjens KB, Heeneman S, et al. In vivo detection of hemorrhage in human atherosclerotic plaques with magnetic resonance imaging. J Magn Reson Imaging 2004;20:105–110.

86. Virmani R, Kolodgie FD, Burke AP, et al. Atherosclerotic plaque progression and vulnerability to rupture: angiogenesis as a source of intraplaque hemorrhage. Arterioscler Thromb Vasc Biol 2005;25:2054–2061.

87. Takaya N, Yuan C, Chu B, et al. Presence of intraplaque hemorrhage stimulates progression of carotid atherosclerotic plaques: a high-resolution magnetic resonance imaging study. Circulation 2005;111:2768–2775.

88. Halcox JP, Schenke WH, Zalos G, et al. Prognostic value of coronary vascular endothelial dysfunction. Circulation 2002;106: 653–658.

89. Targonski PV, Bonetti PO, Pumper GM, Higano ST, Holmes DR Jr, Lerman A. Coronary endothelial dysfunction is associated with an increased risk of cerebrovascular events. Circulation 2003;107:2805–2809.

90. Oliver JJ, Webb DJ. Noninvasive assessment of arterial stiffness and risk of atherosclerotic events. Arterioscler Thromb Vasc Biol 2003;23:554–566.

91. De Vriese AS, Verbeuren TJ, Van de Voorde J, Lameire NH, Vanhoutte PM. Endothelial dysfunction in diabetes. Br J Pharmacol 2000;130:963–974.

92. Zeiher AM, Schachinger V, Minners J. Long-term cigarette smoking impairs endothelium-dependent coronary arterial vasodilator function. Circulation 1995;92:1094–1100.

93. Martin H, Hu J, Gennser G, Norman M. Impaired endothelial function and increased carotid stiffness in 9-year-old children with low birthweight. Circulation 2000;102:2739–2744.

94. Tounian P, Aggoun Y, Dubern B, et al. Presence of increased stiffness of the common carotid artery and endothelial dysfunction in severely obese children: a prospective study. Lancet 2001;358:1400–1404.

95. Wiesmann F, Petersen SE, Leeson PM, et al. Global impairment of brachial, carotid, and aortic vascular function in young smokers: direct quantification by high-reso-

lution magnetic resonance imaging. J Am Coll Cardiol 2004;44:2056–2064.

96. Mohiaddin RH, Firmin DN, Longmore DB. Age-related changes of human aortic flow wave velocity measured noninvasively by magnetic resonance imaging. J Appl Physiol 1993;74:492–497.

97. Rogers WJ, Hu YL, Coast D, et al. Age-associated changes in regional aortic pulse wave velocity. J Am Coll Cardiol 2001;38: 1123–1129.

98. Smits PC, Pasterkamp G, Quarles van Ufford MA, et al. Coronary artery disease: arterial remodelling and clinical presentation. Heart 1999;82:461–464.

99. Varnava AM, Mills PG, Davies MJ. Relationship between coronary artery remodeling and plaque vulnerability. Circulation 2002;105:939–943.

100. Corti R, Fuster V, Fayad ZA, et al. Lipid lowering by simvastatin induces regression of human atherosclerotic lesions: 2 years' follow-up by high-resolution noninvasive magnetic resonance imaging. Circulation 2002;106:2884–2887.

101. Yonemura A, Momiyama Y, Fayad ZA, et al. Effect of lipid-lowering therapy with atorvastatin on atherosclerotic aortic plaques detected by noninvasive magnetic resonance imaging. J Am Coll Cardiol 2005; 45:733–742.

102. Kim WY, Stuber M, Bornert P, Kissinger KV, Manning WJ, Botnar RM. Three-dimensional black-blood cardiac magnetic resonance coronary vessel wall imaging detects positive arterial remodeling in patients with nonsignificant coronary artery disease. Circulation 2002;106:296–299.

103. Koktzoglou I, Simonetti O, Li D. Coronary artery wall imaging: initial experience at 3 tesla. J Magn Reson Imaging 2005;21:128–132.

104. Cappendijk VC, Cleutjens KB, Kessels AG, et al. Assessment of human atherosclerotic carotid plaque components with multisequence MR imaging: initial experience. Radiology 2005;234(2):487–492.

105. Lima JA, Desai MY, Steen H, Warren WP, Gautam S, Lai S. Statin-induced cholesterol lowering and plaque regression after 6 months of magnetic resonance imaging-monitored therapy. Circulation 2004;110:2336–2341.

106. Yarnykh VL, Yuan C. T1-insensitive flow suppression using quadruple inversion-recovery. Magn Reson Med 2002;48:899–905.

107. Takaya N, Yuan C, Chu B, et al. Association between carotid plaque characteristics and subsequent ischemic cerebrovascular events: a prospective assessment with MRI—initial results. Stroke 2006;37(3):818–823.